Time-dependent density-matrix functional theory for trion excitations: Application to monolayer MoS_{2} and other transition-metal dichalcogenides

Alfredo Ramirez-Torres, Volodymyr Turkowski, and Talat S. Rahman

Phys. Rev. B **90**, 085419 — Published 18 August 2014

DOI: 10.1103/PhysRevB.90.085419

Time-dependent density-matrix functional theory for trion excitations: application to monolayer MoS_2 and other transition metal dichalcogenides

Alfredo Ramirez-Torres, Volodymyr Turkowski,* and Talat S. Rahman

Department of Physics, University of Central Florida, Orlando, FL, 32816

*Corresponding author, e-mail address: Volodymyr.Turkowski @ ucf.edu

To examine optically excited bound states , excitons and trions, in monolayer MoS_2, $MoSe_2$ and WSe_2 we have formulated and applied a generalized time-dependent density-matrix functional theory approach. Three different types of exchange-correlation (XC) kernels were used and their validity evaluated through comparison with available experimental data. For excitons, we find that the local kernels, from the local density approximation (LDA) and its gradient-corrected form (GGA), lead to much smaller binding energy than that extracted from experimental data, while those based on long-ranged (LR) interactions fare much better. The same is the case for the trion binding energy , once screening effects are taken into account. Our results suggest that for both excitons and trions the LR form of the XC kernel is necessary to describe bound states. These results confirm information from experimental data on single layer dichalcogenides that their exciton and trion binding energies are of order of hundreds (excitons) and tens (trions) of meVs, a result which may suggest technological application of these materials at room temperature. The proposed methodology can be straightforwardly extended to bound states with larger number of electrons and holes.

PACS numbers:78.67.-n,73.21.b,71.10.-w, 71.15.Mb

I. Introduction

Studies of physical properties of monolayer MoS_2 is a topic of intense research these days, given the multitude of its interesting properties uncovered both experimentally and theoretically.[1-19] These efforts are part of the exploration of new types of two-dimensional materials which potentially extend the fascinating properties of graphene. Although discovered rather recently,[1] this transition-metal chalcogenide system has already recommended itself as a very promising candidate for new nanotechnological applications. In particular, contrary to the case in the bulk, monolayer MoS_2 is a direct band gap semiconductor (with an optical gap of 1.8eV at the K-points in the Brillioun zone) with a very high quantum efficiency for luminescence.[1,2] The system also demonstrates high electron mobility, room-temperature current on/off ratio and ultralow standby power dissipation, with potential to be used in field-effect transistors.[3] It was shown that one can achieve complete dynamic (longer than 1ns) valley polarization in monolayer MoS_2 by

optical pumping with a circularly polarized light.[4,5] Control of the polarization in two direct band gap energy valleys (at K and K' points) could be exploited for applications in valley-based electronic and optoelectronic devices. It is thus not surprising that the optical properties of the system are of special interest, and there is a need for accurate and robust theoretical understanding of excitonic and higher order excited bound states. Experimental data suggests that excitonic effects in the system are large (binding energy ~0.2-1eV).[1,2,6,13] Recently, another exciting property of the MoS_2 monolayer was discovered, namely trion bound state with binding energy approximately 18 meV.[7,9,14] The magnitude of these binding energies suggest both excitonic and trionic effects may have applications at room temperatures. While theoretical studies of excitons in monolayer MoS_2 have already been the subject of several studies (e.g., Refs. 8,9,12,15-19, in which the phenomenological Wannier equation and the GW/Bethe-Salpeter equation (GW/BSE) were used), those of trions are still very few. Using a trial wave function, Berkelbach et al.[12] were able to obtain the binding energies for both these quasi-particles in reasonable agreement with experimental data (though ~30%-over-estimated for trions). It would be difficult, however, to extend their approach to the examination of excitation dynamics. Instead, time-dependent density functional theory (TDDFT) would be a better candidate (see below).

In general, accurate description of bound states and their dynamics in semiconductors is rather messy. Excitons and trions are among the most important of these bound states. Formally, an exciton is defined as a coupled electron-hole pair, while a trion is a bound state of an exciton and

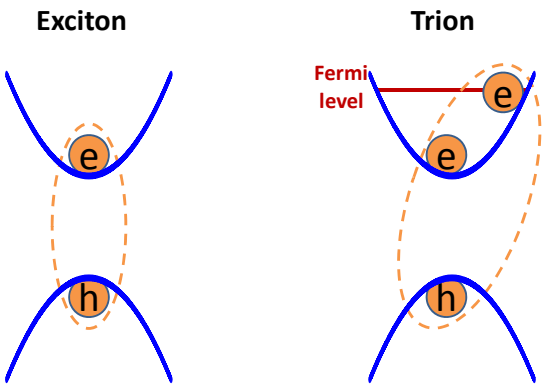

Figure 1. Schematic representation of the quasiparticles, exciton (left) and trion (right), in the two-band model. In the trion case, it is assumed that the exciton (electron-hole pair with energies near the band edges, i.e. with zero total momentum) is coupled to another electron at the Fermi level, the case considered in the paper.

an electron, so the trion can be regarded as a charged exciton (Figure 1). While in bulk systems the trion binding energy is typically negligible compared to that of the exciton, in constrained geometries this energy may be pronounced, leading to novel effects. The most important

example is that of quantum wells, in which trion excitations affect the optical,[10,11] transport[20] and diffusion properties of the system.[21]

Since the standard time-dependent Hartree-Fock approximation leads to strongly over-bound excitonic states, efforts have turned to the development of more subtle many-body methods, such as those based on the GW/BSE approach which take into account screening and other many-particle effects correctly.[22] Unfortunately, such methodology becomes computationally very demanding for calculation of multiple bound states (trions, biexcitons, etc.) and for strongly nonequilibrium processes (for example, ultrafast response of a system), as they require Greens functions with many time arguments. From this point of view, TDDFT[23] is a better candidate. Being a theory of one function – a space- and time-dependent electron charge density, it allows one to get an accurate numerical solution of the system response, provided that the XC potential describing excitonic interactions is available.[24] Some progress in incorporating such effects into TDDFT has already been made. For example, the application of a many-body Greens function[22,25,26] and the exact-exchange approximation.[27,28] However, despite good agreement with experiments, these refinements in TDDFT lead to computational complexities that are almost as demanding as the many-body formalisms. Recently, we have proposed a technically simpler and physically transparent TDDFT approach to study excitonic and biexcitonic effects.[29-31] The approach is based on density-matrix representation of the electron wave-function, and the ensuing generalized TDDFT Bloch equations allow one to calculate excitonic and biexcitonic binding energies using reasonable computational resources. In particular, the exciton equation can be regarded as the TDDFT version of the many-body exciton Wannier equation. We have demonstrated[30,31] that one can obtain rather good agreement with experimental data by choosing proper XC kernel (for example, contact or LR phenomenological kernels).

In this work, we generalize the density-matrix, TDDFT approach to trions and show that the formalism gives rather good agreement with experimental values for the excitonic and trion binding energies for monolayer MoS_2, as well as, for two other members of the monolayer transition-metal dichalcogenide family, $MoSe_2$ and WSe_2, using the same XC potentials.

II. TDDFT for trions

To derive the TDDFT equation for trion binding energy, which we define as the energy necessary to decouple one electron from the coupled electron-hole pair (exciton), we begin with a summary of the density-matrix TDDFT approach for the exciton and biexciton bound states (more details can be found in Refs. 29-31).

a) Excitons. In the case of excitons, one can proceed from the Kohn-Sham equation

$$i\frac{\partial \Psi_{\boldsymbol{k}}^{v}(\mathbf{r},\mathrm{t})}{\partial t} = H(\boldsymbol{r},t)\Psi_{\boldsymbol{k}}^{v}(\boldsymbol{r},t), \qquad (1)$$

where $\boldsymbol{k}$ is the wave vector, v is the valence-band index, and the system Hamiltonian

$$H(\boldsymbol{r},t) = -\frac{\boldsymbol{\nabla}^2}{2m} + V_H[n](\boldsymbol{r},t) + V_{XC}[n](\boldsymbol{r},t) + e\boldsymbol{r}\boldsymbol{E}(t) \quad (2)$$

includes the kinetic (first), Hartree (second) and XC (third) potential terms, as well as, the external homogeneous electric field (the last term). Equation (1) is solved self-consistently with the equation for the electron density, with band index *l*:

$$n(\boldsymbol{r},t) = \sum_{l,|\boldsymbol{k}|<k_F} \left|\Psi_{\boldsymbol{k}}^{l}(\mathbf{r},\mathrm{t})\right|^2. \quad (3)$$

To solve Eqs. (1) and (2) it is convenient to use the density-matrix formalism[29] in which the wave function is expanded in terms of the basis (e.g., Bloch) static wave functions $\psi_{\boldsymbol{k}}^{l}(\boldsymbol{r})$:

$$\Psi_{\boldsymbol{k}}^{v}(\mathbf{r},\mathrm{t}) = \sum_{l} c_{\boldsymbol{k}}^{vl}(t)\psi_{\boldsymbol{k}}^{l}(\boldsymbol{r}), \quad (4)$$

The time-dependent coefficients $c_{\boldsymbol{k}}^{vl}(t)$ completely describe the system dynamics. Below we drop index *v* for sake of simplicity, since we will consider the case of one valence band. Coefficients can be found from the following equation:

$$i\frac{\partial \mathrm{c}_{\boldsymbol{k}}^{m}}{\partial t} = \sum_{l} \mathrm{H}_{\boldsymbol{k}\boldsymbol{k}}^{ml}\mathrm{c}_{\boldsymbol{k}}^{l}, \quad (5)$$

where

$$H_{\boldsymbol{k}\boldsymbol{q}}^{lm}(t) = \int \psi_{\boldsymbol{k}}^{l*}(\boldsymbol{r})H[n](\boldsymbol{r},t)\psi_{\boldsymbol{q}}^{m}(\boldsymbol{r})d\boldsymbol{r}. \quad (6)$$

However, to study the system response it is more convenient to consider the bilinear combination of *c*-coefficients, the density matrix:

$$\rho_{\boldsymbol{k}\boldsymbol{q}}^{lm}(t) = c_{\boldsymbol{k}}^{l}(t)c_{\boldsymbol{q}}^{m*}(t). \quad (7)$$

Its diagonal elements describe the level occupancies, while the non-diagonal – electron transitions, including excitonic effects. The matrix elements satisfy the Liouville equation:

$$i\frac{\partial \rho_{\boldsymbol{k}\boldsymbol{q}}^{lm}(\mathrm{t})}{\partial t} = [H(t),\rho(t)]_{\boldsymbol{k}\boldsymbol{q}}^{lm}. \quad (8)$$

In the case of two (valence *v* and conduction *c*) bands, one can derive the exciton TDDFT equation for the non-diagonal element $\rho_{\boldsymbol{k}\boldsymbol{q}}^{cv}(t)$ by using Eqs. (2), (3),(7) and (8). Expansion of the charge density fluctuations in (8) in terms of the density matrix elements (6) (by using Eq. (3)) leads to the TDDFT Wannier equation:[30]

$$\left[\left(\varepsilon^{c}_{\boldsymbol{k+q}}-\varepsilon^{v}_{\boldsymbol{k}}\right)\delta_{\boldsymbol{kk'}}+F^{cvvc}_{\boldsymbol{kkk'k'}}\right]\rho^{cv}_{n,\boldsymbol{k'}+\alpha\boldsymbol{q}}(\omega)=E_{n,\boldsymbol{q}}\,\rho^{cv}_{n,\boldsymbol{k}+\alpha\boldsymbol{q}}, \tag{9}$$

where $\boldsymbol{q}$ is the exciton momentum, α is the reduced hole mass, and n is the bound state number. The effective electron-hole interaction is described by the last matrix elements defined as:

$$F^{abcd}_{\boldsymbol{kqk'q'}}(\omega)=\int d\boldsymbol{r}_1 d\boldsymbol{r}_2\,\psi^{a*}_{\boldsymbol{k}}(\boldsymbol{r}_1)\psi^{b}_{\boldsymbol{q}}(\boldsymbol{r}_1)f_{XC}(\boldsymbol{r}_1,\boldsymbol{r}_2,\omega)\psi^{c*}_{\boldsymbol{k'}}(\boldsymbol{r}_2)\psi^{d}_{\boldsymbol{q'}}(\boldsymbol{r}_2). \tag{10}$$

With $\boldsymbol{q}$=0 one can obtain the excitonic binding energies from Eq. (9).

b) Biexcitons. Similarly, one can consider the two-electron TDDFT problem in order to derive the equation for biexcitonic states.[31] In TDDFT language, this is a problem of two excited electrons in the field of two holes. The corresponding equation is

$$i\frac{\partial\Psi^{vv}_{\boldsymbol{k}_1\boldsymbol{k}_2}(\boldsymbol{r}_1,\boldsymbol{r}_2,\mathrm{t})}{\partial t}=\left[H(\boldsymbol{r}_1,t)+H(\boldsymbol{r}_2,t)+\frac{1}{|\boldsymbol{r}_1-\boldsymbol{r}_2|}\right]\Psi^{vv}_{\boldsymbol{k}_1\boldsymbol{k}_2}(\boldsymbol{r}_1,\boldsymbol{r}_2,\mathrm{t}), \tag{11}$$

where the single-electron Hamiltonian is defined in Eq.(2), while the last term in brackets on the right hand side describes electron-electron repulsion. The two-particle wave function can be expanded in terms of two single-electron functions:

$$\Psi^{vv}_{\boldsymbol{k}_1\boldsymbol{k}_2}(\boldsymbol{r}_1,\boldsymbol{r}_2,\mathrm{t})=\sum_{l,m}B^{lm}_{\boldsymbol{k}_1\boldsymbol{k}_2}(t)\psi^{l}_{\boldsymbol{k}_1}(\boldsymbol{r}_1)\,\psi^{m}_{\boldsymbol{k}_2}(\boldsymbol{r}_2), \tag{12}$$

where the two-electron matrix elements satisfy:

$$i\frac{\partial \mathrm{B}^{cd}_{\boldsymbol{k}_1\boldsymbol{k}_2}}{\partial t}=\sum_{a,\boldsymbol{p}}\left[\mathrm{H}^{ca}_{\boldsymbol{k}_1\boldsymbol{p}}\mathrm{B}^{ad}_{\boldsymbol{p}\boldsymbol{k}_2}+\mathrm{H}^{da}_{\boldsymbol{k}_2\boldsymbol{p}}\,\mathrm{B}^{ca}_{\boldsymbol{k}_1\boldsymbol{p}}\right]+\sum_{a,b,\boldsymbol{p}_1,\boldsymbol{p}_2}\mathrm{w}^{cdab}_{\boldsymbol{k}_1\boldsymbol{k}_2\boldsymbol{p}_1\boldsymbol{p}_2}\mathrm{B}^{ab}_{\boldsymbol{p}_1\boldsymbol{p}_2}, \tag{13}$$

with $\mathrm{H}^{ca}_{\boldsymbol{kp}}$ defined in Eq. (7) and

$$\mathrm{w}^{cdab}_{\boldsymbol{k}_1\boldsymbol{k}_2\boldsymbol{p}_1\boldsymbol{p}_2}=\frac{1}{\varepsilon_{ee}}\int d\boldsymbol{r}_1 d\boldsymbol{r}_2\,\psi^{c*}_{\boldsymbol{k}_1}(\boldsymbol{r}_1)\psi^{d*}_{\boldsymbol{k}_2}(\boldsymbol{r}_2)\frac{1}{|\boldsymbol{r}_1-\boldsymbol{r}_2|}\psi^{a}_{\boldsymbol{p}_1}(\boldsymbol{r}_1)\psi^{b}_{\boldsymbol{p}_2}(\boldsymbol{r}_2) \tag{14}$$

is the matrix element that corresponds to electron-electron repulsion (ε_{ee} is an effective electron-electron screening parameter). Similar to the excitonic case, in order to get biexciton eigen-energies one can consider a linearized form of the corresponding Equation (13). Indeed, if the lowest eigen-energy of this equation is smaller than the sum of two exciton energies obtained from Eq. (9) this means that two excitons form a bound state.

c) Trions. In a similar way one can study the case of a trion - two excited electrons described by the field $B^{ab}_{\boldsymbol{k}_1\boldsymbol{k}_2}(t)$ in presence of the hole $c^{c*}_{\boldsymbol{q}}(t)$. The corresponding matrix element

$$\mathrm{t}^{abc}_{\boldsymbol{k}_1\boldsymbol{k}_2\boldsymbol{q}}(t)=\mathrm{B}^{ab}_{\boldsymbol{k}_1\boldsymbol{k}_2}(t)c^{c*}_{\boldsymbol{q}}(t) \tag{15}$$

defines the time-dependence of the three-particle wave function:

$$\Psi^{v}_{\boldsymbol{k}_1\boldsymbol{k}_2\boldsymbol{q}}(\boldsymbol{r}_1,\boldsymbol{r}_2,\boldsymbol{r}_3,\mathrm{t}) = \sum_{l,m} t^{lmn}_{\boldsymbol{k}_1\boldsymbol{k}_2\boldsymbol{q}}(t)\psi^{l}_{\boldsymbol{k}_1}(\boldsymbol{r}_1)\,\psi^{m}_{\boldsymbol{k}_2}(\boldsymbol{r}_2)\psi^{n*}_{\boldsymbol{q}}(\boldsymbol{r}_3) \tag{16}$$

(the trion excitation corresponds to the upper index *lmn=ccv*). Using Eqs.(5) and (13), one can obtain the following equation for the three-particle density matrix:

$$i\frac{\partial \mathrm{t}^{abc}_{\boldsymbol{k}_1\boldsymbol{k}_2\boldsymbol{q}}}{\partial t} = \sum_{f,\boldsymbol{p}}\left[\mathrm{H}^{af}_{\boldsymbol{k}_1\boldsymbol{p}}\mathrm{t}^{fbc}_{\boldsymbol{p}\boldsymbol{k}_2\boldsymbol{q}} + \mathrm{H}^{bf}_{\boldsymbol{k}_2\boldsymbol{p}}\,\mathrm{t}^{afc}_{\boldsymbol{k}_1\boldsymbol{p}\boldsymbol{q}} - \mathrm{H}^{fc}_{\boldsymbol{p}\boldsymbol{q}}\mathrm{t}^{abf}_{\boldsymbol{k}_1\boldsymbol{k}_2\boldsymbol{p}}\right] + \sum_{f,m,\boldsymbol{p}_1,\boldsymbol{p}_2} \mathrm{w}^{abfm}_{\boldsymbol{k}_1\boldsymbol{k}_2\boldsymbol{p}_1\boldsymbol{p}_2}\mathrm{t}^{fmc}_{\boldsymbol{p}_1\boldsymbol{p}_2\boldsymbol{q}}, \tag{17}$$

where the H- and w-matrix elements are defined in Eqs. (6) and (14), correspondingly. Linearization of this equation gives the equation for the trion eigen-energies:

$$\begin{aligned} i\frac{\partial \mathrm{t}^{ccv}_{\boldsymbol{k}_1\boldsymbol{k}_2\boldsymbol{q}}}{\partial t} &= \left(\varepsilon^{c}_{\boldsymbol{k}_1} + \varepsilon^{c}_{\boldsymbol{k}_2} - \varepsilon^{v}_{\boldsymbol{q}}\right)\mathrm{t}^{ccv}_{\boldsymbol{k}_1\boldsymbol{k}_2\boldsymbol{q}} \\ &+ \sum_{\boldsymbol{p}_1,\boldsymbol{p}_2}\left[\mathrm{F}^{cvvc}_{\boldsymbol{k}_1\boldsymbol{q}\boldsymbol{p}_2\boldsymbol{p}_1}\mathrm{t}^{ccv}_{\boldsymbol{p}_1\boldsymbol{k}_2\boldsymbol{p}_2} + \mathrm{F}^{cvvc}_{\boldsymbol{k}_2\boldsymbol{q}\boldsymbol{p}_2\boldsymbol{p}_1}\mathrm{t}^{ccv}_{\boldsymbol{k}_1\boldsymbol{p}_1\boldsymbol{p}_2} + \mathrm{w}^{cccc}_{\boldsymbol{k}_1\boldsymbol{k}_2\boldsymbol{p}_1\boldsymbol{p}_2}\mathrm{t}^{ccv}_{\boldsymbol{p}_1\boldsymbol{p}_2\boldsymbol{q}}\right], \end{aligned} \tag{18}$$

were $\varepsilon^{c}_{\boldsymbol{k}}$ and $\varepsilon^{v}_{\boldsymbol{k}}$ are the free-electron and free-hole spectra, and F and w potentials describe the TDDFT electron-hole and electron-electron scattering (in particular, the first two F-terms, respectively, describe the scattering of the first electron with momentum $\boldsymbol{k}_1$ on the hole with momentum $\boldsymbol{q}$, and similarly the second F-term describes the scattering of the first and second electron with momenta $\boldsymbol{k}_1$ and $\boldsymbol{k}_2$ on the hole with momentum $\boldsymbol{q}$).

Eqs. (9), (10), (14) and (18) suggest a way of generalization of the corresponding eigen-energy equations for excitations with larger number of bound electrons and holes than the trion. One would apply a many-particle Schroedinger equation such as (18), in which electrons and holes attract each other with the potentials, or rather scattering matrix elements F (Eq.(10)), while the electron-electron and hole-hole repulsion potentials are defined by matrix elements w as in Eq.(14). Thus, each pair of electrons interact through the TDDFT scattering potential:

$$\mathrm{w}^{cccc}_{\boldsymbol{k}\boldsymbol{q};\boldsymbol{k}'\boldsymbol{q}'} = \frac{1}{\varepsilon_{ee}}\int d\boldsymbol{r}_1 d\boldsymbol{r}_2\,\psi^{c*}_{\boldsymbol{k}}(\boldsymbol{r}_1)\psi^{c*}_{\boldsymbol{q}}(\boldsymbol{r}_2)\frac{1}{|\boldsymbol{r}_1-\boldsymbol{r}_2|}\psi^{c}_{\boldsymbol{k}'}(\boldsymbol{r}_1)\psi^{c}_{\boldsymbol{q}'}(\boldsymbol{r}_2), \tag{19}$$

which describes the scattering of two electrons with momenta $\boldsymbol{k}$, $\boldsymbol{q}$ to the states with momenta $\boldsymbol{k}'$ and $\boldsymbol{q}'$. Similarly, one can describe the corresponding hole-hole scattering by changing all band indices from "*c*" to "*v*" in the last equation. The electron-hole attraction is described by the scattering potential

$$\mathrm{F}^{cvvc}_{\boldsymbol{k}\boldsymbol{q};\boldsymbol{k}'\boldsymbol{q}'} = \int d\boldsymbol{r}_1 d\boldsymbol{r}_2\,\psi^{c*}_{\boldsymbol{k}}(\boldsymbol{r}_1)\psi^{v}_{\boldsymbol{q}}(\boldsymbol{r}_2)f_{XC}(\boldsymbol{r}_1,\boldsymbol{r}_2)\psi^{c}_{\boldsymbol{k}'}(\boldsymbol{r}_1)\psi^{v*}_{\boldsymbol{q}'}(\boldsymbol{r}_2), \tag{20}$$

which similarly describes the scattering of the electron-hole pair from the state with momenta $\boldsymbol{k}$ and $\boldsymbol{q}$ to the state with momenta $\boldsymbol{k}'$ and $\boldsymbol{q}'$. For example, in the case of biexciton (two electrons with momenta $\boldsymbol{k}_1$ and $\boldsymbol{k}_2$ and two holes with momenta $\boldsymbol{q}_1$ and $\boldsymbol{q}_2$) the corresponding equation for the "wave function" $\mathrm{B}^{ccvv}_{\boldsymbol{k}_1\boldsymbol{k}_2\boldsymbol{q}_1\boldsymbol{q}_2}$ has the following form:

$$
\begin{aligned}
i\frac{\partial \mathrm{B}^{ccvv}_{\boldsymbol{k}_1\boldsymbol{k}_2\boldsymbol{q}_1\boldsymbol{q}_2}}{\partial t} = {} & \left(\varepsilon^{c}_{\boldsymbol{k}_1} + \varepsilon^{c}_{\boldsymbol{k}_2} - \varepsilon^{v}_{\boldsymbol{q}_1} - \varepsilon^{v}_{\boldsymbol{q}_2}\right)\mathrm{B}^{ccvv}_{\boldsymbol{k}_1\boldsymbol{k}_2\boldsymbol{q}_1\boldsymbol{q}_2} \\
& + \sum_{\boldsymbol{k},\boldsymbol{q}} \left[\mathrm{F}^{cvvc}_{\boldsymbol{k}_1\boldsymbol{q}_1\boldsymbol{q}\boldsymbol{k}}\mathrm{B}^{ccvv}_{\boldsymbol{k}\boldsymbol{k}_2\boldsymbol{q}\boldsymbol{q}_2} + \mathrm{F}^{cvvc}_{\boldsymbol{k}_1\boldsymbol{q}_1\boldsymbol{q}\boldsymbol{k}}\mathrm{B}^{ccvv}_{\boldsymbol{k}\boldsymbol{k}_2\boldsymbol{q}_1\boldsymbol{q}} + \mathrm{F}^{cvvc}_{\boldsymbol{k}_2\boldsymbol{q}_1\boldsymbol{q}\boldsymbol{k}}\mathrm{B}^{ccvv}_{\boldsymbol{k}_1\boldsymbol{k}\boldsymbol{q}\boldsymbol{q}_2} + \mathrm{F}^{cvvc}_{\boldsymbol{k}_2\boldsymbol{q}_2\boldsymbol{q}\boldsymbol{k}}\mathrm{B}^{ccvv}_{\boldsymbol{k}_1\boldsymbol{k}\boldsymbol{q}_1\boldsymbol{q}}\right] \\
& + \sum_{\boldsymbol{p}_1,\boldsymbol{p}_2} \left[\mathrm{w}^{cccc}_{\boldsymbol{k}_1\boldsymbol{k}_2\boldsymbol{p}_1\boldsymbol{p}_2}\mathrm{B}^{ccvv}_{\boldsymbol{p}_1\boldsymbol{p}_2\boldsymbol{q}_1\boldsymbol{q}_2} + \mathrm{w}^{vvvv}_{\boldsymbol{q}_1\boldsymbol{q}_2\boldsymbol{p}_1\boldsymbol{p}_2}\mathrm{B}^{ccvv}_{\boldsymbol{k}_1\boldsymbol{k}_2\boldsymbol{p}_1\boldsymbol{p}_2}\right]. \qquad (21)
\end{aligned}
$$

This equation has to be compared with the standard Schrödinger equation for two electrons and two holes:

$$
\begin{aligned}
i\frac{\partial \Psi_{\boldsymbol{k}_1\boldsymbol{k}_2\boldsymbol{q}_1\boldsymbol{q}_2}}{\partial t} = {} & \left(\varepsilon^{c}_{\boldsymbol{k}_1} + \varepsilon^{c}_{\boldsymbol{k}_2} - \varepsilon^{v}_{\boldsymbol{q}_1} - \varepsilon^{v}_{\boldsymbol{q}_2}\right)\Psi_{\boldsymbol{k}_1\boldsymbol{k}_2\boldsymbol{q}_1\boldsymbol{q}_2} \\
& - \sum_{\boldsymbol{k}} \frac{1}{\boldsymbol{k}^2}\left[\Psi_{\boldsymbol{k}\boldsymbol{k}_2-\boldsymbol{k}\boldsymbol{q}_2} + \Psi_{\boldsymbol{k}\boldsymbol{k}_2\boldsymbol{q}_1-\boldsymbol{k}} + \Psi_{\boldsymbol{k}_1\boldsymbol{k}-\boldsymbol{k}\boldsymbol{q}_2} + \Psi_{\boldsymbol{k}_1\boldsymbol{k}\boldsymbol{q}_1-\boldsymbol{k}}\right] \\
& + \sum_{\boldsymbol{p}_1,\boldsymbol{p}_2} \frac{1}{\boldsymbol{k}^2}\left[\Psi_{\boldsymbol{k}-\boldsymbol{k}\boldsymbol{q}_1\boldsymbol{q}_2} + \Psi_{\boldsymbol{k}_1\boldsymbol{k}_2\boldsymbol{k}-\boldsymbol{k}}\right]. \qquad (22)
\end{aligned}
$$

While the solution of this equation might be not less complicated than the solution of the corresponding many-body equation, the main advantage of the TDDFT approach is inclusion of many-body effects through the two-particle attraction defined, in principle, by an exact XC kernel. This property is especially important in the strongly non-equilibrium regime with multiple excitations, in which non-linear effects must be taken into account.

III. Excitons and trions in monolayer MoS_2, $MoSe_2$ and WSe_2

III.a The method

To calculate exciton and trion binding energies, we generate the Kohn-Sham eigenfunctions and eigenenergies using the DFT code Quantum-ESPRESSO,[32] and employ the BEE (Binding Energies of Excitons) code developed in our group to obtain the necessary parameters and to solve the exciton and trion eigenenergy equations (9) and (18). At the DFT stage, exchange and correlation effects are included by applying the local density approximation (LDA) in the Perdew and Zunger parametrization.[33] In these calculations, we used norm conserving pseudo-

potentials[34] and a cut off energy of 60 Ry and a 15x15x1 ***k***-point grid to represent the reciprocal space.[35] To model single layers of transition metal dichalcogenides, as shown in Figure 2, we used a supercell with (1x1) periodicity and ~15 Å of vacuum between periodic images. The calculated lattice parameter *a* is 3.167, 3.289, 3.244Å for monolayer of MoS_2, $MoSe_2$, WSe_2 respectively. In the non-self-consistent calculations of the relaxed single-layer structures we used 48x48x1 ***k***-point grid (217 independent ***k***-points in the first Brillouin zone).

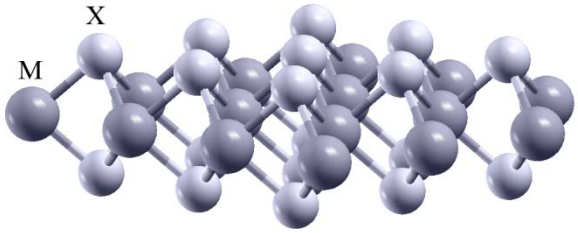

Figure 2. Structure of monolayer transition metal dichalcogenides MX_2 (M = Mo, W; X = S, Se).

The results of the band structure calculations for MoS_2 are presented in Fig.3.

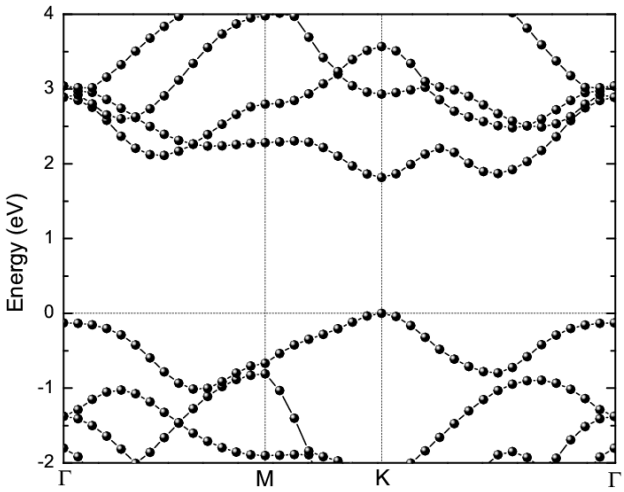

Figure 3. Band structure of monolayer MoS_2 calculated with LDA.

Despite the standard underestimation of the bandgap by LDA, our results (1.82, 1.59, 1.72 eV for MoS_2, $MoSe_2$, WSe_2, respectively) are in a reasonable agreement with experimental estimations of the optical bandgap.[1,36] While this agreement between the LDA and experimental results might be regarded as fortuitous, more accurate approaches that take into account screening

effects, such as the HSE hybrid functional calculations, provide results that indeed agree rather well with experimental data (HSE gives the direct gap ~2.2eV[37] for MoS_2). On the other hand, the absolute value of the gap is not critical for purposes here, since the binding energy is calculated with respect to the conduction band edge.

To calculate the exciton and trion binding energies we solve equations (9) and (18) using the following eight kernels (details of which can be found in Ref. 17 and references therein):

- Three local kernels: the first consists of phenomenological contact interaction $f_{XC}^{local}(\boldsymbol{r},\boldsymbol{r}') = -4\pi A\delta(\boldsymbol{r}-\boldsymbol{r}')$, where A is a parameter describing the strength of the TDDFT local electron-hole attraction; the other two are based on LDA: 1) with exchange (X) only; 2) with both exchange and correlation (XC). These kernels allow us to examine how correlation, as incorporated in LDA, affects binding energies. Note that the contact kernel with A=1 is the two-dimensional (2D) LDA(X) kernel (even though MoS_2 is not exactly a 2D system, application of this kernel to it may help provide insights into how spatial constrains affect bound state energies).

- Three gradient-corrected kernels: gradient-expansion approximation (GEA), and two with the Generalized Gradient Approximation (GGA) (PW91[38] and PBE[39]). These kernels take into account the effects of possible strong spatial variation of the electronic charge, and hence the spatial-dependence of the local electron-hole interaction, which may be rather important in the monolayer systems with spatially-constrained charge.

- Two LR kernels: phenomenological $f_{XC}(\boldsymbol{r},\boldsymbol{r}') = -\frac{1}{\varepsilon}\frac{1}{|\boldsymbol{r}-\boldsymbol{r}'|}$, where ε is an effective screening of the electron-hole attraction, and the Slater kernel (optimized effective potential (OEP) case[40]) with physically correct electron-hole interaction, which includes a Coulomb singularity.

III.b. Excitons

There is no total agreement on the values of the exciton binding energies in monolayer MoS_2, $MoSe_2$ and WSe_2 in the community. Thus, while combined DFT-based phenomenological modeling approach[15] and GW-Bethe-Salpeter Equation (GW-BSE)[16-19] calculations predict extremely large binding energies for the excitons in MoS_2 (0.54eV and 0.5-1.03eV, correspondingly), experimental scanning tunneling microscopy/spectroscopy (STM/S) and photoluminescence (PL) analysis[13] suggests that the corresponding energy is approximately 0.22eV (or 0.42eV when some additional assumptions on the interpretation of the experimental data are taken into account). Similar, in the $MoSe_2$ case computational analysis[15,16] shows some difference between the calculated exciton energies and the ones obtained within theSTM/STS+PL spectroscopy studies[41] (0.47eV and 0.91eV vs. 0.55eV). Berkelbach et al.[15] and Ramasubramaniam[16] also performed calculations of the exciton energy for WSe_2 to obtain exciton binding energy of 0.45eV and 0.9eV, respectively, which are again overestimate the spectroscopically measured value of 0.37eV.[42] The results for the binding energy of excitons for the systems of interest, calculated with the above kernels, are presented in Tables I-III and Figs. 4 and 5. In the case of MoS_2, we find that the contact kernel can reproduce experimentally estimated energy 0.3eV[13] at A=0.238. We also find that the exciton binding energy is very

sensitive to the value of A (Table I and Figure 4). To test the ability of contact kernel to describe excitons in other transition metal dichalcogenides, we extended our calculations to single layer $MoSe_2$ and WSe_2. As shown in Fig. 4, the values of A for the three different dichalcogenides are very similar (~0.2-0.4). Taking into account the oversimplification in the contact approximation this result is quite remarkable.

On one hand, LDA with either X or XC gives very small binding energies (~1-10meV, Table III). Comparing this result to that obtained for the contact kernel, and taking into account the fact that the required A is of order 1 (2D LDA), one can suggest that indeed the spatial constraint in one direction may be important for excitons in these system. On the other hand, very small decrease of the LDA binding energy with inclusion of the correlations suggests that it is not very important in these materials (though the situation may change dramatically when one dopes the system with transition metal atoms). We also found that charge-gradient correction does not improve the situation significantly. The GEA and PW91 binding energies are even lower than LDA ones. Though PBE gives much larger energies than LDA, it is still much lower than the experimental values. It is also worthwhile to note that the LDA and GGA exciton energies for the $MoSe_2$ are an order of magnitude larger than that for other two materials, which display very similar values. The d-states of the Se atoms with more localized charge densities may be playing a role here.

Table I. Exciton binding energy (in meV) for monolayer MoS_2 calculated with the contact kernel for different values of coupling parameter A.

A	1	0.5	0.395	0.238	0.213	0.1	exp
E_X	3,863	1,494	1,000	300	200	1	220-420

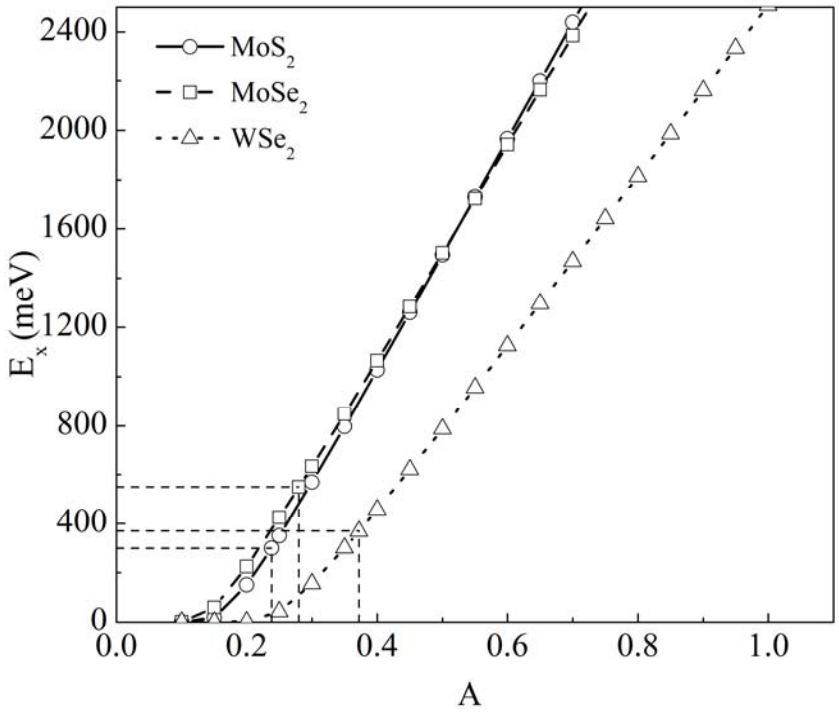

Figure 4. Exciton binding energy (in meV) calculated with the contact kernel for different values of coupling parameter A for monolayer MoS_2, $MoSe_2$ and WSe_2. The dashed lines mark the experimental values for E_x (see Refs. [13,41,42]) and the corresponding As.

Table II. Exciton binding energy (in meV) calculated with seven remaining kernels for the three materials. In the case of LDA both X and XC results are presented, while in the GEA, PW91 and PBE cases only the X result is shown. For LR, we use the screening parameter $\varepsilon = 1$.

	LDA(X)	LDA(XC)	GEA	PW91	PBE	LR	Slater	exp.
MoS_2	2.05	2.00	0.87	1.96	10.46	90.54	1,093	220-420[13]
$MoSe_2$	14.81	14.45	1.21	12.58	39.34	187	1,183	550[41]
WSe_2	1.20	1.19	0.53	1.63	2.25	9.81	734	370[42]

The results for the exciton binding energy change dramatically when one takes into account the Coulomb nature of the interaction (a kernel with $\frac{1}{q^2}$ singularity (see, e.g., Refs. [27-29])). While the unscreened ($\varepsilon = 1$) phenomenological LR kernel gives underestimated values of the binding energy (Table III, Figure 5), the Slater kernel results are in a reasonable agreement with the experiment [13,41,42] and other calculations[15-19] (Table II). In the LR case, the results are very sensitive to the value of the screening parameter ε, and one can obtain the experimental energy by lowering the screening parameter by ~20 percent to the vacuum (unscreened) value. Interestingly, similar to the local case, the value of the fitting (screening) parameter has the same

order of magnitude in all three cases (Fig. 5). On the other hand, it seems problematic to get accurate experimental binding energy if one uses experimentally motivated values of the screening parameter. In particular, in the case of MoS_2, the parallel and perpendicular components of the dielectric constant are $\varepsilon_{\parallel}$=2.8 and $\varepsilon_{\perp} = 4.2$ (Ref. [8]), and their average is $\bar{\varepsilon} = \sqrt{\left(2\varepsilon_{\parallel}^2 + \varepsilon_{\perp}^2\right)/3} \approx 3.3$, which corresponds also to the dielectric constant of bulk MoS_2 (Ref. [43]). E_X is extremely sensitive to the value of screening at $0.5 < \varepsilon < 3 - 4$ (Table III, Fig. 5). It suggests that this potential will result in an accurate description of the exciton effects when used as a part of a hybrid potential, for example with one of GGAs

Table III. Exciton binding energy for MoS_2 (in meV) for the LR kernel and different values of ε.

ε	0.449	0.752	0.844	1	2.8	4.2	3.3	exp.
E_X	1,000.00	300	200	90.54	0.62	0.39	0.51	220-420[13]

It must be emphasized that in our calculations we do not include spin-orbital band splitting whose inclusion would have resulted in two exciton peaks (the band splitting is much smaller than the exciton and trion excitation energies). The inclusion of spin-orbit effects is, however, straightforward. Namely, in this case one needs to consider two split valence bands, which will transform the exciton and trion equations (9) and (18) into 2×2 matrix equations (in the band indices). The band splitting will lead to two exciton peaks separated by approximately the band-splitting energy.

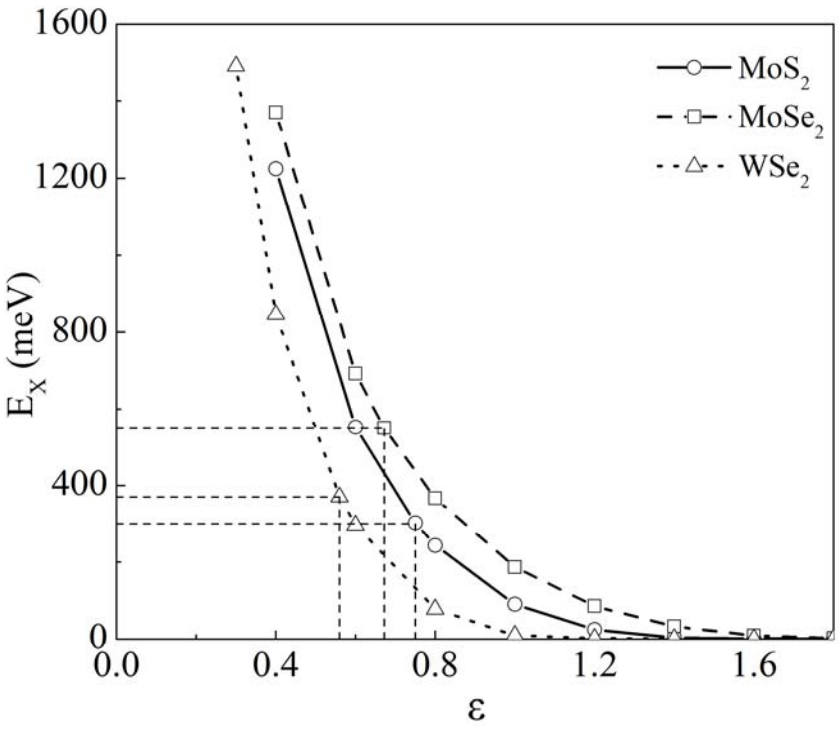

Figure 5. Exciton binding energy (in meV) for the LR kernel and different values of ε for the three materials. The corresponding experimental values[13,41,42] are marked by dashed lines.

III.c. Trions

Equation (18) for the trion energy is rather complicated to be solved exactly, therefore we use an approximation, similar to the many-body case. Namely, it is convenient to reduce the problem to that of an electron with momentum $\boldsymbol{k}_1$ in the presence of an exciton comprised of the remaining electron and hole (momenta $\boldsymbol{k}_2$ and **q)**. In this case, using Eq.(9) for the exciton function, one can transform Eq.(18) to

$$i\frac{\partial \mathrm{t}^{ccv}_{\boldsymbol{k}_1\boldsymbol{k}_2\boldsymbol{q}}}{\partial t} = \left(\varepsilon^{c}_{\boldsymbol{k}_1} + E_{X\,\boldsymbol{k}_2,\boldsymbol{q}}\right)\mathrm{t}^{ccv}_{\boldsymbol{k}_1\boldsymbol{k}_2\boldsymbol{q}} + \sum_{\boldsymbol{p}_1,\boldsymbol{p}_2}\left[\mathrm{F}^{cvvc}_{\boldsymbol{k}_1\boldsymbol{q}\boldsymbol{p}_2\boldsymbol{p}_1}\mathrm{t}^{ccv}_{\boldsymbol{p}_1\boldsymbol{k}_2\boldsymbol{p}_2} + \mathrm{w}^{cccc}_{\boldsymbol{k}_1\boldsymbol{k}_2\boldsymbol{p}_1\boldsymbol{p}_2}\mathrm{t}^{ccv}_{\boldsymbol{p}_1\boldsymbol{p}_2\boldsymbol{q}}\right]. \qquad (23)$$

Next, we assume that the excitonic electron and hole momenta are fixed, $\boldsymbol{k}_2 = \boldsymbol{q}$, i.e. we consider the exciton with fixed center-of-mass. The trion equation now reduces to

$$i\frac{\partial \mathrm{t}^{ccv}_{\boldsymbol{k}_1\boldsymbol{q}\boldsymbol{q}}}{\partial t} = \left(\varepsilon^{c}_{\boldsymbol{k}_1} + E_{X\,\boldsymbol{q},\boldsymbol{q}}\right)\mathrm{t}^{ccv}_{\boldsymbol{k}_1\boldsymbol{q}\boldsymbol{q}} + \sum_{\boldsymbol{p}_1,\boldsymbol{p}_2}\left[\mathrm{F}^{cvvc}_{\boldsymbol{k}_1\boldsymbol{q}\boldsymbol{q}\boldsymbol{p}_1}\mathrm{t}^{ccv}_{\boldsymbol{p}_1\boldsymbol{q}\boldsymbol{q}} + \mathrm{w}^{cccc}_{\boldsymbol{k}_1\boldsymbol{q}\boldsymbol{p}_1\boldsymbol{q}}\mathrm{t}^{ccv}_{\boldsymbol{p}_1\boldsymbol{q}\boldsymbol{q}}\right] = 0, \qquad (24)$$

which is equivalent to the following eigen-energy equation:

$$\left(\varepsilon_{\boldsymbol{k}}^{c} + E_{X\,\boldsymbol{q},\boldsymbol{q}} - \omega\right)\delta_{\boldsymbol{kp}} + \mathrm{F}_{\boldsymbol{kqqp}}^{cvvc} + \mathrm{w}_{\boldsymbol{kqpq}}^{cccc} = 0. \quad (25)$$

We assume that exciton is created in one of two equivalent **K**-points, which correspond to the direct bandgap transition, and put $\boldsymbol{q}$ equal to the **K**-point momentum. While it is easy to generalize the solution to arbitrary exciton momenta, the trion energy obtained with this approximation is sufficient to estimate the energy scale of the trionic effects in the system, including the position of the trion peak in the optical absorption spectrum.

Before presenting our results for the trion binding energy, we summarize the experimental data known to us for the three systems. Absorption and PL (MoS_2),[14] differential reflectance and PL ($MoSe_2$)[44] and PL (WSe_2)[45] measurements give ~18meV (MoS_2) and ~30meV ($MoSe_2$ and WSe_2) as the trion binding energies. The results of the solution of Eq. (25) using the contact kernel with A=0.238 (the case of characteristic exciton energy 0.3eV) at different values of the electron-electron screening for MoS_2 are summarized in Figure 6. Clearly, the results are very sensitive to the value of ε, though one can successfully reproduce the experimental result 18meV[14] at a reasonable value $\varepsilon \sim 11$. We did not find a finite binding energy when using the LDA, GEA and GGA kernels, a naturally expected result because of the extremely low excitonic energies obtained from these kernels (see Table II, where all the results for the local kernels are summarized). The results in Tables I and II suggest that while the TDDFT exciton energies can be obtained by assuming even a local electron-hole attraction, to get a bound state of an electron and an exciton one needs to take into account the long-range character of the interaction (long-range interaction also reproduce correct exciton energies). Indeed, the electron-exciton interaction is more of "a dipole" type, contrary to the Coulomb interaction of the electron and hole. As for excitons, the fact that the contact kernel (2D LDA) results in a finite trion binding energy, contrary to that for the bulk with LDA, suggests that the spatial constraint (charge non-homogeneity) of the system is important in this case too. We find very similar results for the trion energy for the other two single layer dichalcogenides by using the local attraction and screened Coulomb repulsion (Figure 6). In particular, the value of the screening parameter necessary to reproduce correct trion energy has the same order of magnitude for all three materials.

Table IV. The trion binding energy for MoS_2 (in meV) in the case of contact kernel with A=0.395 and different values of the electron-electron screening parameter ε_{ee}. The corresponding exciton energy is 1,093meV.

ε_{ee}	2.8	3.3	4	4.146	4.2	4.5	5	exp.
E_T	0	0.15	1.74	20	31.7	105	223	18[14]

In the case of LR kernels, we find that the trion energy is sensitive to the value of the electron-electron screening. In particular, for MoS_2 one can easily reproduce the experimental binding energy with the Slater kernel at fair value $\varepsilon \sim 2.7$ (Table V). Similar results were found for the other two materials, with the close values for the fitting screening parameter (Fig. 7).

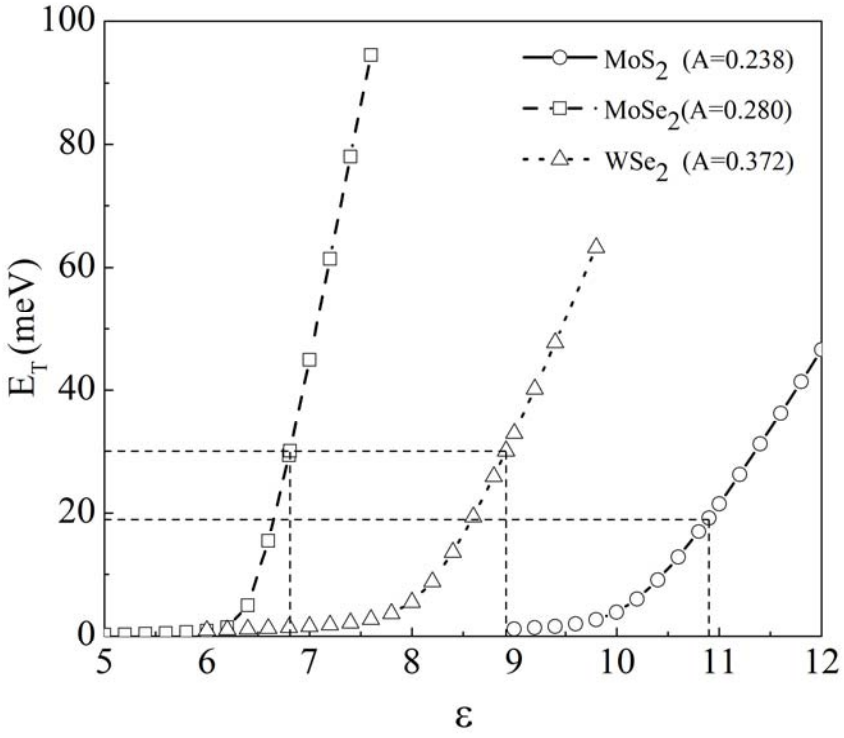

Figure 6. The trion binding energy (in meV) obtained with the contact kernel (with A corresponding to exciton energy of 300, 550, 370 meV for MoS_2, $MoSe_2$, WSe_2, respectively) at different values of the electron-electron screening parameter ε_{ee}. Again the corresponding experimental values are marked by dashed lines.

Table V. The trion binding energy in MoS_2 (in meV) obtained with the Slater kernel and different values of the electron-electron screening parameter. The corresponding exciton energy is 1,093meV.

ε	1	2.7874	2.8	3.3	4.2	exp
E_T	0	20	27	293	642	18[14]

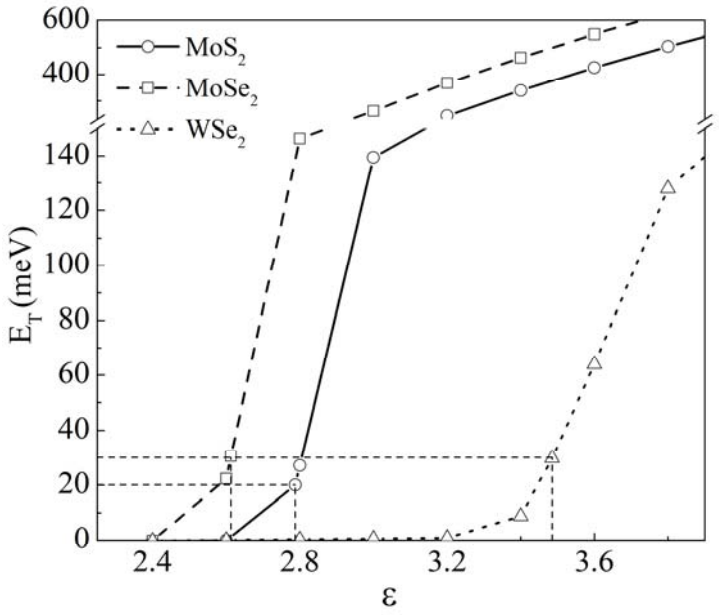

Figure 7. The trion binding energy (in meV) obtained with the Slater kernel and different values of the electron-electron screening parameter for the three materials. The dashed lines correspond to experimental values.[12]

IV. Conclusions

In this work, we have formulated a density-matrix TDDFT approach to examine the energies of trions in bulk systems, as well as, in nano-materials. This approach is physically transparent, with the inter-particle interaction defined by the TDDFT XC kernel. Similar to the formalism for excitons, this methodology has several advantages over standard many-body approaches – simplicity and accurately accounting of many-body correlation (especially screening) effects.

We applied the approach to study exciton and trion binding energies in monolayer MoS_2, $MoSe_2$ and WSe_2. There are experimental indications that the corresponding binding energies in these materials are rather large (~0.2-0.5eV[13,41,42] and 0.02-0.03eV[14,44,45]), which makes it possible to use the exciton and trion effects at room temperatures. We show a theoretical confirmation of these high binding energies when we employ a long-range Slater XC kernel, which takes into account correctly the nature of the electron-hole interaction. We find some phenomenological kernels (one LR and one contact) with physically reasonable values of parameters to also provide reasonable binding energies. On the other hand, we find that for both excitons and trions

one cannot obtain finite (non-negligible) values with standard LDA and GGA kernels, as a results of the missing long-ranged nature of the electron-hole interaction. The reasonable agreement with experimental values for three different monolayer transition metal dichalcogenides suggests the universality of the proposed potentials.

The formalism described above can be used to study binding energies and ultrafast processes that involve excitonic, trionic and biexcitonic effects. The scheme proposed in the paper can be easily generalized to bound states with larger number of quasi-particles.

Acknowledgements

We thank Tony Heinz for many helpful conversations. This work was financially supported in part by US Department of Energy (DE-FG02-07ER46354). A.R.T. would like to acknowledge CONACYT (Mexico) for support through the Postdoctoral Fellowship Program (No. 184722).

References:

1. K.F. Mak, C. Lee, J. Hone, J. Shan, and T.F. Heinz, Phys. Rev. Lett. **105**, 136805 (2010).
2. A. Splendiani, L. Sun, Yu. Zhang, T. Li, J. Kim, C.-Y. Chim, G. Galli, and F. Wang, Nano Lett. **10**, 1271 (2010).
3. B. Radisavljevic, A. Radenovic, J. Brivio, V. Giacometti and A. Kis, Nature Nanotech. **6** , 147 (2011).
4. K.F. Mak, K. He, J. Shan and T.F. Heinz, Nature Nanotech. **7**, 494 (2012).
5. H. Zeng, J. Dai, W. Yao, D. Xiao and X. Cui, Nature Nanotech. **7**, 490 (2012).
6. R. S. Sundaram, M. Engel, A. Lombardo, R. Krupke, A.C. Ferrari, Ph. Avouris, M. Steiner, Nanoletters **13**, 1416 (2013).
7. K.F. Mak, K. He, C. Lee, G.H. Lee, J. Hone, T.F Heinz, and J. Shan, Nature Mat. 12, 207 (2013).
8. T. Cheiwchanchamnangij and W.R.L. Lambrecht, Phys. Rev. B **85**, 205302 (2012).
9. A. Ramasubramaniam, Phys. Rev. B **86**, 115409 (2012).
10. M. T. Portella-Oberli, V. Ciulin, J. H. Berney, B. Deveaud, M. Kutrowski and T. Wojtowicz, Phys. Rev. B **69**, 235311 (2004).
11. V. Ciulin, P. Kossacki, S. Haacke, J.-D. Ganière, B. Deveaud A. Esser, M. Kutrowski and T. Wojtowicz, Phys. Rev. B **62**, R16310 (2000).
12. T.C.Berkelbach, M.S. Hybertsen, and D.R. Reichman, Phys. Rev. B 88, 045318 (2013).
13. C. Zhang, A. Johnson, C.-L. Hsu, L.-J. Li, C.-K. Shih, Nano Lett. **14**, 2443 (2014).
14. K.F. Mak, K.L. He, C. Lee, G.H. Lee, J. Hone, T.F. Heinz, J. Shan, Nat. Mater. **12**, 207 (2013).
15. T.C. Berkelbach, M.S. Hybertsen, and D.R. Reichman, Phys. Rev. B 88, 045318 (2013).
16. A. Ramasubramaniam, Phys. Rev. B 86, 115409 (2012).
17. H.-P. Komsa and A.V. Krasheninnikov, Phys. Rev. B 86, 241201(R) (2012).

18. J. Feng, X. Qian, Ch.-W. Huang and J. Li, Nat. Photonics 6, 866 (2012).
19. H. Shi, H. Pan, Y.-W. Zhang, and B.I. Yakobson, Phys. Rev. B 87, 155304 (2013).
20. D. Sanvitto, F. Pulizzi, A.J. Shields, P.C.M. Christianen, S.N. Holmes, M.Y. Simmons, D.A. Ritchie, J.C. Maan, M. Pepper, Science **294**, 837 (2001).
21. M.T. Portella-Oberli, V. Ciulin, S. Haacke, J.-D. Ganière, P. Kossacki, M. Kutrowski, T. Wojtowicz, and B. Deveaud, Phys. Rev. B **66**, 155305 (2002).
22. G. Onida, L. Reining, A. Rubio, Rev. Mod. Phys. **74**, 601 (2002).
23. E. Runge and E.K.U. Gross, Phys. Rev. Lett. **52**, 997 (1984).
24. C.A. Ullrich, "Time-Dependent Density-Functional Theory: Concepts and Applications" (Oxford University Press, 2012).
25. L. Reining, V. Olevano, A. Rubio, and G. Onida, Phys. Rev. Lett. **88**, 066404 (2002).
26. A. Marini, R. Del Sole, and A. Rubio, Phys. Rev. Lett. **91**, 256402 (2003).
27. Y.H. Kim and A. Görling, Phys. Rev. Lett. **89**, 096402 (2002).
28. Y. H. Kim and A. Görling, Phys. Rev. B **66**, 035114 (2002).
29. V. Turkowski, C.A. Ullrich, Phys. Rev. B **77**, 075204 (2008).
30. V. Turkowski, A. Leonardo, C.A. Ullrich, Phys. Rev. B **79**, 233201 (2009).
31. V. Turkowski, C.A. Ullrich, T.S. Rahman, and M.N. Leuenberger, Phys. Rev. B **82**, 205208 (2010).
32. S. Baroni, A. Dal Corso, S. de Gironcoli, P. Giannozzi, C. Cavazzoni, G. Ballabio, S. Scandolo, G. Chiarotti, P. Focher, A. Pasquarello, K. Laasonen, A. Trave, R. Car, N. Marzari, A. Kokalj, (http://www.pwscf.org/).
33. J. P. Perdew, A. Zunger, Phys. Rev. B **23**, 5048 (1981).
34. N. Troullier, J. L. Martins, Phys. Rev. B **43**, 1993 (1991).
35. H.J. Monkhorst, J. D. Pack, Phys. Rev. B **13**, 5188 (1976).
36. S. Tongay, J. Zhou, C. Ataca, K. Lo, T. S. Matthews, J. Li, J. C. Grossman, and J. Wu, Nano Lett. **12**, 5576 (2012).
37. J.K. Ellis, M.J. Lucero, and G.E. Scuseria, Appl. Phys. Lett. **99**, 261908 (2011).
38. J.P. Perdew, K. Burke, and M. Ernzerhof, Phys. Rev. Lett. 77, 3865 (1996).
39. J.P. Perdew, in "Electronic Structure of Solids 1991", ed. by P. Ziesche, H. Eschrig (Akademie Verlag, Berlin, 1991), p. 11.
40. C.A. Ullrich, U.J. Gossmann and E.K.U. Gross, Phys. Rev. Lett. 74, 872 (1995).
41. M.M. Ugeda, A.J. Bradley, S.-F. Shi, F.H. da Jornada, Y. Zhang, D.Y. Qiu, S.-K. Mo, Z. Hussain, Z.-X. Shen, F. Wang, S.G. Louie, M.F. Crommie, preprint arXiv:1404.2331v1 (2014).
42. K. He, N. Kumar, L. Zhao, Z. Wang, K.F. Mak, H. Zhao, J. Shan, preprint arXiv:1406.3095v1 (2014).
43. Y. Yoon, K. Ganapathi, S. Salahuddin, Nano Lett. **11**, 3768 (2011).
44. J.S. Ross, S.F. Wu, H.Y. Yu, N.J. Ghimire, A.M. Jones, G. Aivazian, J.Q. Yan, D.G. Mandrus, D. Xiao, W. Yao, X.D. Xu, Nat. Commun. **4**, 1474 (2013).

45. A.M. Jones, H. Yu, N.J. Ghimire, S. Wu, G. Aivazian, J.S. Ross, B. Zhao, J. Yan, D.G. Mandrus, D. Xiao, W. Yao and X. Xu, Nat. Nanotech. **8**, 634 (2013).